Ind. J. Pharm. Edu. Res., 2026; 60(2s):s687-s698.
https://www.ijper.org

Original Article

Experimental Research of Ions in Wound Healing Via Film Forming Solution

Ketura Kambampaty[1], Nagesh Chandrashekhar Setty[1], Suma Naduvinamani[1,*], Kartik Bhairu Khot[1], Sibghatullah Muhammad Ali Sangi[2], Sreeharsha Nagaraja[3], Girish Meravanige[4], Mohammed Monirul Islam[5,*], Pavan Kumar Sreenivasalu[6], Shahzad Chohan[5]

[1]Department of Pharmaceutics, Maratha Mandal's College of Pharmacy, Belagavi, Karnataka, INDIA.
[2]Basic Medical Sciences Department, College of Medicine, Dar al Uloom University, Riyadh, SAUDI ARABIA.
[3]Department of Pharmaceutical Sciences, College of Clinical Pharmacy, King Faisal University, Al-Ahsa, SAUDI ARABIA.
[4]Department of Biomedical Sciences, College of Medicine, King Faisal University, Al-Ahsa, SAUDI ARABIA.
[5]Department of Biomedical Sciences, College of Clinical Pharmacy, King Faisal University, Al-Ahsa, SAUDI ARABIA.
[6]Department of Restorative Dentistry and Endodontics, College of Dentistry, King Faisal University, Al-Ahsa, SAUDI ARABIA.

ABSTRACT

Objectives: This study aimed to investigate the wound healing potential of Film Forming Solution (FFS) incorporated with Silver (Ag) and Copper Oxide (CuO) Nanoparticles (NPs). **Materials and Methods:** Ag NPs were synthesized by chemical reduction and CuO NPs by the co-precipitation method and optimized for concentration, pH, and temperature. Characterization was performed using UV-vis spectroscopy, FT-IR, particle size analysis, zeta potential, and SEM. Antibacterial activity was assessed by determining the MIC against *Staphylococcus aureus* and *Escherichia coli*. Optimized NPs were incorporated into a polymeric FFS and evaluated for various physicochemical properties. *In vivo* wound healing studies were carried out in Wistar rats for 21 days, and histopathological examinations were conducted to assess tissue regeneration. **Results:** Ag NPs exhibited a Surface Plasmon Resonance (SPR) peak at 432 nm with an average size of 72.61 nm, while CuO NPs showed strong absorption at 262.5 nm with a size of 105.5 nm. Zeta potential values were –27.3 mV for Ag NPs and –10.2 mV for CuO NPs, suggesting moderate colloidal stability. SEM revealed spherical, clustered Ag NPs and irregularly shaped CuO NPs. MIC values displayed broad spectrum activity of these NPs. *In vivo* wound healing studies revealed that control animals achieved 91.67 ± 0.88% wound closure, blank FFS-treated animals 83.44 ± 0.80%, standard-treated animals 99.44 ± 0.11%, Ag-FFS 99.0 ± 0.19%, and CuO-FFS 98.89 ± 0.22%. **Conclusion:** These findings highlight their potential as advanced topical delivery systems for safe and effective wound management.

Keywords: Copper oxide, Film-forming solution, Nanoparticles, Silver, Wound healing.

Correspondence:
Dr. Suma Naduvinamani
Associate Professor, Department of Pharmaceutics, Maratha Mandal's College of Pharmacy, Rajiv Gandhi University of Health Sciences, Belgaum-590016, Karnataka, INDIA.
Email: suma4u_q12@yahoo.co.in

Dr. Mohammed Monirul Islam
Department of Biomedical Sciences, College of Clinical Pharmacy, King Faisal University, Al-Ahsa 31982, SAUDI ARABIA.
Email: mislam@kfu.edu.sa

Received: 22-07-2025;
Revised: 14-11-2025;
Accepted: 11-12-2025.

INTRODUCTION

The skin is the human body's largest organ. The fundamental role of the skin is to protect the underlying tissues and organs from mechanical pressures, infections, fluid imbalance, and heat dysregulation.[1] A wound is defined as any physical injury to the body that disturbs the normal structure and function of the skin.[2] Wounds are a major global health concern; about 3 to 4 out of every 1000 people in Denmark and the United Kingdom have one or more wounds. Many of these wounds develop into long-term injuries, and sadly, 15% of wounds fail to recover within a year after occurrence.[3] Wound healing is a complicated process that aims to restore injured skin and maintain tissue homeostasis. It requires the interaction of several cell types, growth hormones, cytokines, and a steady supply of metal ions including calcium, zinc, and magnesium.[4] Numerous studies have demonstrated that the direct or indirect regulation of certain metal ions is associated with wound healing.[5]

Silver (Ag) ion has been used historically to cure burns and wounds, cleanse water, and treat a variety of illnesses and infections. Because its ions are active and may pass through bacterial membranes, silver functions as an antimicrobial. Ag ions have been shown to accelerate wound healing and to be highly effective even at low concentrations.[6] Copper (Cu), due to its well-established antibacterial characteristics, makes a significant component in wound healing, skin remodeling, and anti-inflammatory therapy.[7] Since free metal ions can have harmful consequences in biological medium, thus its usual practice to transform them into well-designed nanoparticles to

DOI: 10.5530/ijper.20264372

increase stability, decrease ion release and cytotoxicity, and allow for more regulated administration.[8]

Nanotechnology provides a variety of novel approaches to regenerative medicine. Nanomaterials improve delayed wound healing and burn therapy. Dressings containing Ag NPs are safe to use for lengthy periods of time.[9] Cu deficiency is known to slow wound healing. Wounds treated with NPs-free ointments required 14 days to fully heal, but those treated with Cu NPs containing ointments healed two days sooner.[10,11] When NPs are used topically, they help wounds heal more cosmetically and offer a useful therapeutic approach for scarless wound healing.[12] These days, wound care includes cleaning, disinfecting, dressing, and, if necessary, closing the wound. Every wound dressing should provide the ideal criteria for healing such as infection control, waste and debris clearance, enough oxygenation, and a moist environment that promotes cell migration and wound closure.[13] The ideal dressing should have qualities like good mechanical strength, flexibility, non-toxicity, and biodegradability. It should also be biocompatible, functioning as a physical barrier against microorganisms while permitting air permeation to keep the wound hydrated and remove excess exudates. The novel Film Forming Solution (FFS) possesses all these attributes.[14]

The principle of film-forming formulations is somewhat new. Film-forming formulations might be solutions, gels, or emulsions. FFS are non-solid dosage forms that create a significant film *in situ* following application to the skin or any other bodily surface. The generated film is substantial enough to offer prolonged medication release to the skin.[15] Films serve as handy physical barriers to germs, retain gas permeability, and allow for *in situ* medication delivery. Furthermore, their adaptability may be modified to match individual morphology. Films can maintain ideal wound repair conditions by keeping the area wet, eliminating wound exudates, and speeding up cellular and tissue regeneration.[13]

Therefore, in the present work, Ag and Cu ions are converted into Ag NPs and CuO NPs, and characterized for various parameters. Then the optimized NPs were incorporated into FFS, and their potential to accelerate wound healing was assessed.

MATERIALS AND METHODS

Materials

The chemicals used were of analytical grade. Ag Nitrate ($AgNO_3$) was obtained from Oxford Laboratory, Mumbai. Cupric Sulphate pentahydrate ($CuSO_4.5H_2O$) was obtained from Molychem, Mumbai. Sodium Hydroxide (NaOH), Hydroxy Propyl Cellulose (HPC) and Triethyl citrate were purchased from SD Fine-Chem Ltd, Mumbai. Polyvinylpyrrolidone K25 (PVP) and Ethanol were obtained from Loba Chemie, Mumbai, while Eudragit L 100 was procured from Yarrow Pharma, Mumbai.

Methods

Synthesis of Ag NPs

Ag NPs were synthesized via a chemical reduction method using PVP as a stabilizing agent and NaOH as a pH adjuster. In a typical procedure, a specified amount of PVP (1.5%) was dissolved in deionized water under constant stirring. Once the PVP was fully dissolved, an aqueous solution of NaOH (0.1M) was added dropwise to the mixture to adjust the pH and initiate the alkaline environment required for the reduction process. After stabilization of the solution, 5 mM $AgNO_3$ solution was slowly added dropwise under continuous stirring. The entire reaction proceeded at 60°C until a visible color change (pale yellow) indicated the formation of Ag NPs. The resulting colloidal solution was further stirred for 30 min to ensure no change in color, complete reduction and stabilization of the NPs.[16]

Synthesis of CuO NPs

The co-precipitation method was used to create CuO NPs. This special synthesis involved dissolving 0.1 M $CuSO_4.5H_2O$ in 100 mL of deionized water and continuously stirring the mixture until a homogenous blue solution was formed. After adding 0.2 M NaOH, the mixture was stirred at 80°C for 2 hr to produce a black precipitate, which was thereafter allowed to cool to room temperature. After precipitation, the starting material was eliminated by filtering and washing the precipitate with more methanol. For further characterization, the powder was lastly dried for 4 hr at 300°C in a hot air oven.[17]

Characterization of Ag NPs and CuO NP

Ultraviolet-visible spectral analysis

The initial color change of the reaction mixture indicates the formation of NPs. Further, it is confirmed by the reading absorbance in the visible range of 200-800 nm. To confirm the formation of NPs, absorbance is read using a UV-visible spectrophotometer (Shimadzu UV-1900i) in the wavelength range 200-800 nm.[18]

Fourier Transform Infrared Spectroscopy (FT-IR)

FT-IR was performed to know the chemical environment of the NPs and the excipients used in the formulation. FT-IR analysis of Ag NPs and CuO NPs was characterized using Alpha II Bruker FT-IR spectrophotometer, in the range of 400-4000 cm^{-1}.[19]

Particle size and Zeta Potential analysis

The particle size distribution, particle size, and zeta potential of synthesized Ag NPs and CuO NPs were determined by the DLS technique using a Malvern Zeta-sizer and HORIBA SZ-100 instrument. The NPs were uniformly dispersed in Milli Q water using an ultrasonic bath operated at 40kHz for 1 min at room temperature. [20]

Scanning electron microscope

The morphology/shape of the Ag NPs and CuO NPs was studied through a scanning electron microscope (JSM-IT810, JEOL Ltd, Japan) with a resolution of 60A^0 at 15kV magnification of 5.[21]

Minimum Inhibitory Concentration

The resazurin assay technique was used to assess the antimicrobial activity of the synthesized test sample. The experiment was conducted by dissolving 270 mg of resazurin in 40 mL of sterile distilled water. A vortex mixer was employed to ensure that the solution was homogeneous and thoroughly dissolved. The tests were carried out using a 96-well plate under aseptic conditions. To begin, pipette 100 µL of varying concentrations of dimethyl sulphoxide (7.8, 15.6, 31.2, 62.5, 125, 250, 500, 1000 µg/mL) into the plate well. Then, 50 µL of nutritional broth was poured into each well and then diluted. In each well, 10 µL of resazurin indicator solution was used. Following that, 10 µL of fungal or bacterial solution was applied to each well. Streptomycin (7.8, 15.6, 31.2, 62.5, 125, 250, 500, 1000 µg/mL) served as a standard control. To prevent microorganisms from drying out, each plate was lightly wrapped with cling film. The plate was then incubated for 18-24 hr at 37°C, and the color change was observed visually. Any color changes from blue to pink or colorless were designated as positive, while the absence of color shift was indicated as negative. The absorbance of the plate was measured at 600 nm using an ELISA reader. The percentage of inhibition was calculated by following the formula:[22]

$$\% \text{ of Inhibition} = \left(\frac{\text{Test}}{\text{Control}}\right) * 100$$

Preparation of FFS containing Ag NPs and CuO NPs

Eudragit L 100 was sprinkled over 10 mL of ethanol along with triethyl citrate, whereas HPC was sprinkled over a separate 10 mL of ethanol. To get clear solutions, both mixtures were left to swell for a whole day. The polymeric solutions were adequately blended with continuous stirring. The NPs solution in ethanol and polymeric dispersion were thoroughly mixed with continuous stirring, and the volume was brought up to the mark with ethanol (Table 1). [23]

Evaluation of FFS

Drying time

After the solution is sprayed, the film's drying time is measured to determine how quickly the film forms. The solution is sprayed over the surface of the glass under certain conditions and allowed to dry at room temperature and the drying time was directly measured. A glass plate is placed against the film without being moved in order to check if it has dried. The film is deemed dry if there is no water adhesion to the glass.[24]

Film flexibility

The film was taken from the mold and tested for flexibility by bending, rolling, and twisting. Flexibility was defined as the ability to bend the film without breaking or fracturing.[25]

Thickness

A vernier caliper was used to measure the thickness of the film. The whole length of the film was measured at five separate locations in the middle and on the sides, and the mean results were converted to the film thickness in microns.[26]

Viscosity determination

The Brookfield viscometer (Brookfield Engineering Laboratories, USA) was used to test viscosity by choosing spindle numbers 64 and 50 rpm. The process was carried out three times, and the mean of the observations was noted.[27]

pH determination

A digital pH meter (Servewell Instruments Pvt. Ltd., India) was used to measure the FFS's pH. The pH value was measured by immersing the electrode in the FFS.[28]

Folding Endurance

The film was folded repeatedly from the same spot before breaking to test folding endurance.[29]

In vivo Wound healing study

Wound healing activity using animal model

Animal studies were performed with prior approval from the Institutional Animal Ethics Committee of Maratha Mandal's College of Pharmacy (MMCP/2024-25/B.Ph/218). Total of 24 Wistar albino rat model was used to carry out the wound-healing activities. The following five groups (n = 3) were created from adult rats weighing 150-200 g: Group 1 was a control group that was injured and given saline solution treatment; Group 2 was a marketed product that was treated with Ag sulfadiazine; Group 3 was blank FFS; Group 4 was formulated FFS that contained Ag NPs; and Group 5 was formulated FFS that contained CuO NPs. Each rat's dorsal region was shaved with an electric trimmer the day before the experiment. Using forceps and surgical scissors,

Table 1: Formulation of FFS.

Ingredients	Quantity for FFS containing Ag NPs (Ag FFS)	Quantity for FFS containing CuO NPs (CuO FFS)
NPs	25% (v/v)	0.05% (w/v)
Eudragit L 100 (w/v)	12.5	12.5
HPC (w/v)	2	2
Triethyl citrate	0.93	0.93
Ethanol	Quantity sufficient	Quantity sufficient

excision were made on the dorsal spinal area after anesthesia was established using the open-mask technique with anesthetic ether. An appropriate amount of FFS was applied daily on the wound throughout the study period. Following the application, each rat was kept in a cage at room temperature. Four weeks later, the damaged skin tissue was removed, stored in 10% formalin, and examined histopathologically.[30]

Determination of wound contraction

The wound area in the excision wound model was calculated by tracing the wound on millimeter-based graph paper on days 7, 14, and 21 for every group. Wound contraction was measured and reported as a percentage (%) of the healed wound area every seven days until complete wound healing was seen. The percentage of wound contraction was computed using the formula.[30]

$$\%\ Wound\ Contraction: \frac{(initial\ wound\ area - specific\ wound\ area)}{Initial\ wound\ area} * 100$$

Determination of epithelialization period

The epithelization period was defined as the time needed to remove the dead tissue without leaving any raw wounds behind. This was thought to be the final point of full epithelization.[30]

Histopathology

Histopathology of wounds is a very helpful tool to assess physical changes, follow healing progress throughout therapy, understand the epidemiology of non-healing wounds, track the origin of a disease, and aid in diagnosis. Because it enables comparison of the ulcerated area with the surrounding skin, the outermost layer of the lesion is the best place for a biopsy in clinical settings. In the lab, a sample of the whole wound, including the margins, was taken for histological analysis. Tissue samples were submerged in certain solutions as soon as they were collected, such as 10% buffered formalin, one of the most used fixatives, to maintain their integrity and avoid changes to the cellular structure. After that, the tissue was processed for staining, sectioning, and embedding.[31]

Statistical analysis

The experiments were carried out in triplicate (n=3) and the average values with their standard error are provided in this publication. A result of $p < 0.05$ was considered significant.[32]

Stability studies

The ICH criteria were followed for conducting the stability investigations for the film forming solution. The product was exposed to 4 ± 2°C, 25 ± 2°C, and 40°C ± 2°C, and 75% ± 5 relative humidity for three months. The polymeric solution's viscosity, pH, and physical characteristics were assessed.[33]

RESULTS

Visual Observation

The formation of Ag NPs was visually observed from the change in the color of the solution from colorless to pale yellow, which on further stirring changed to reddish. The formation of CuO NPs was visually observed from the change in the color of the solution from bluish green to blackish precipitate.

UV Spectroscopy

Figure 1 (A, B) shows the absorption spectra of Ag NPs and CuO NPs. A strong plasmon resonance peak was recorded in the UV area, around 432 nm, indicating the production of Ag NPs. The most significant absorption of CuO NPs produced via chemical

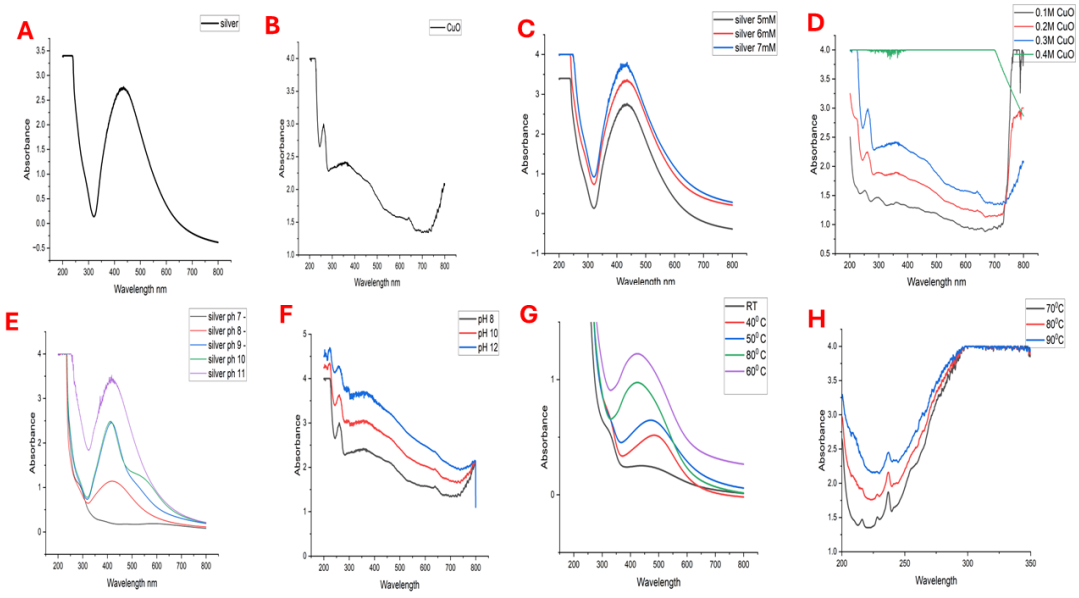

Figure 1: UV peak of (A) Ag NPs (B) CuO NPs; Effect of Concentration (C) Ag NPs (D) CuO NPs; Effect of pH (E) Ag NPs (F) CuO NPs; Effect of Temperature (G) Ag NPs (H) CuO NPs.

precipitation was discovered to be at 262.5 nm. The spectroscopic data clearly showed the formation of Ag NPs and CuO NPs.

Optimization of NPs

In the current study, various parameters such as salt concentration, pH of the reaction mixture and temperature were optimized because these parameters have desirable control over morphological characteristics such as particle size and shape, as well as influence NPs production yield. As a result, these characteristics must be optimized during the NPs manufacturing process.

Effect of concentration

The concentration of $AgNO_3$ is a key parameter that influences the shape and yield of NPs. The current work investigated the appropriate quantity of Ag salt necessary for the synthesis of Ag NPs at varied concentrations of $AgNO_3$ (5 mM, 6 mM, and 7 mM) while maintaining a constant temperature of 60 °C and pH of 9**.** Figure 1 (C) shows the UV spectrum of the effect of various $AgNO_3$ concentrations.

Absorption spectra were used to characterize the optical properties of CuO NPs at different concentrations of $CUSO_4.5H_2O$ (0.1M, 0.2M, 0.3M, and 0.4M). The absorption spectra of CuO NPs at 0.3 M exhibit a strong peak at 252.5 nm due to direct electron transition. The absorption band was at 261.5 nm for 0.2 M and 262 nm for 0.1 M concentrations, but there was no peak at 0.4 M, as shown in Figure 1 (D).

Effect of pH

The pH of the reaction mixture is also a crucial parameter since it influences the size, shape, and stability of NPs. In the current work, the influence of pH on the synthesis of Ag NPs was evaluated at neutral and basic pH media (pH 7, 8, 9, 10, and 11) while maintaining a constant temperature of 60°C, and the observed UV spectrum is shown in Figure 1 (E).

The absorbance spectra of produced CuO NPs at pH 8, 10, and 12 are shown in Figure 1 (F). According to the data, no shift in the peak was seen, with the exception of variations in peak strength as pH increased. The peak intensity dropped as the pH increased from 8 to 12.

Effect of temperature

Temperature is taken into account, and synthesis of Ag NPs was conducted at various temperatures (room temperature, 40°C, 50°C, 60°C, and 80°C). Figure 1 (G) shows the UV spectra of the effect of temperature, and it was found that the peak shifts slightly towards a shorter wavelength from 479 nm to 435.5 nm and that the peak intensity increases with increasing temperature.

Figure 1 (H) shows the UV-Vis absorption spectra of CuO NPs synthesized at 70°C, 80°C, and 90°C, revealing a strong relationship between optical characteristics on synthesis temperature. As the temperature increased, so did the total absorbance intensity, with the greatest absorbance recorded at 90°C.

FT-IR

The spectra of the Ag NP, shown in Figure 2 (A), reveal a very strong peak at 3324.28 cm^{-1}, which is related to the free OH group present in the reduction agent for Ag^+ to Ag^0. The steep peak at 1636.40 cm^{-1} corresponds to C=O group vibrations, whilst the C-O stretching may be detected at 2112.40 cm^{-1}. The existence of OH molecules and C=O groups can also be explained by the reduction process, which produces these isomers.[34] The FT-IR spectra of CuO samples generated using the co-precipitation

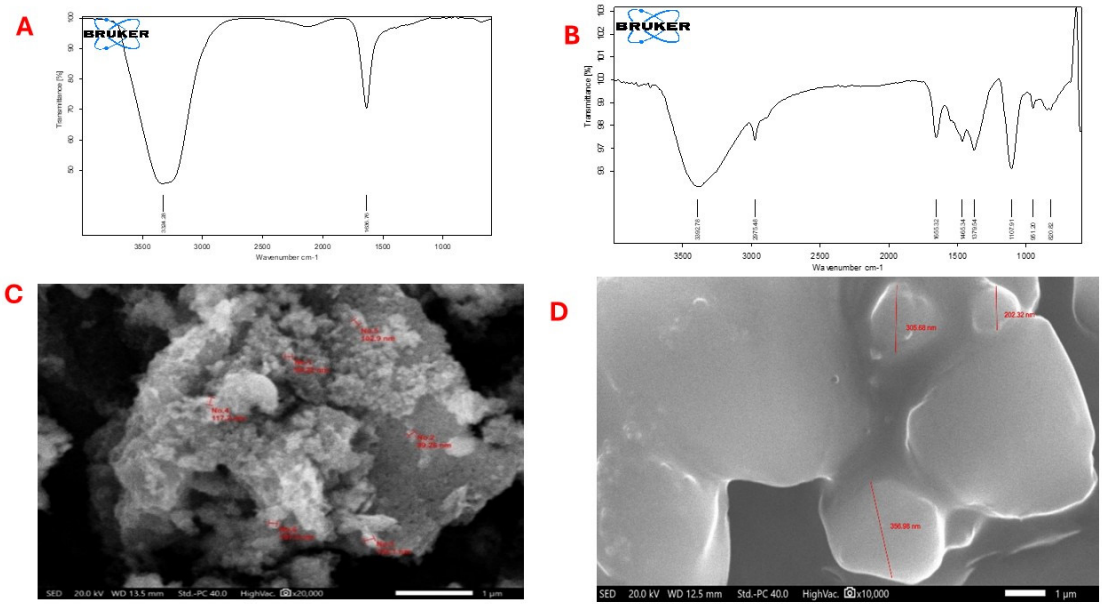

Figure 2: FT-IR spectra of (A) Ag NP (B) CuO NPs; SEM images of (C) Ag NP (D) CuO NPs.

technique are displayed in Figure 2 (B). CuO spectra are categorized into three regions: 600–1100 cm^{-1}, 1300-1700 cm^{-1}, and 2800–3700 cm^{-1}. The distinctive peaks at 820.62 cm^{-1}, 952.20 cm^{-1}, and 1107.91 cm^{-1}, seen between 600 and 1100 cm^{-1}, are connected with the Cu-O stretching mode. Similarly, peaks in the second area 1300-1700 cm^{-1}, might indicate the presence of CO_2. The third zone, which ranges from 2800 to 3700 cm^{-1}, is caused by water and hydrated CuO.[35]

Particle size and zeta potential

The average particle size, size distribution, and Polydispersity Index (PDI) values for Ag NPs and CuO NPs was determined by Dynamic Light Scattering technique. The Z-average diameter of synthesized Ag NP and CuO NPs was 72.61 nm and 105.5 nm, with a PDI of 0.479 and 0.480, respectively. The zeta potential of Ag NPs and CuO NPs, were determined to be -27.3 mV and -10.2 mV, respectively.

Scanning Electron Microscopy (SEM)

Scanning electron microscopy has been proven to be a unique approach for analyzing the morphological characteristics of nanostructures. Figure 2 (C, D) shows SEM images of Ag and CuO NP morphology.

Minimum Inhibitory Concentration (MIC)

The MIC of Ag NP and CuO NPs was determined against two bacterial strains: *Staphylococcus aureus* and *Escherichia coli*. The MIC values represent the lowest concentration of the compounds at which the test pathogen did not develop visibly. The MIC for Ag NPs was 31.2 µg/mL for *S. aureus* and 62.5 µg/mL for *E. coli*, whereas CuO NPs had a MIC of 62.5 µg/mL for both bacteria.

Evaluation of film forming solution

Film formation

Both the FFS after been formulated, a small volume of sample was poured onto the glass slab to determine how the film forms. Both the formed films were complete, dried, opaque and easily peelable. The outcomes of the film formation are recorded in Table 2.

Drying time

The Ag FFS dries in 3.17±0.07 min, while the CuO FFS takes 3.20±0.14 min. Table 2 gives the drying times for each formulation.

Film flexibility

Due to their strong attachment ability and lack of breaking, the resulting films from both formulations were flexible. Table 2 contains a tabulation of the results.

Thickness

Table 2 lists the thicknesses of the manufactured films. The data indicate that as the polymer concentration increases, so does the film's thickness. The thickness of Ag FFS film was 0.17±0.03 mm, while CuO FFS was 0.18±0.01 mm.

Viscosity determination

The Brookfield viscometer was used to determine the viscosity of Ag FFS and CuO FFS. The viscosity of Ag FFS was 8.1±0.05 cps of viscosity, while the CuO FFS had 8.2±0.01. Table 2 presents the findings.

Table 2: Evaluation of film forming solution.

Formulation code	Ag FFS	CuO FFS
Film formation	Complete, Dried, Opaque, Peelable	Complete, Dried, Opaque, Peelable
Drying time (minutes)	3.17±0.07	3.20±0.14
Film flexibility	flexible	flexible
Thickness (mm)	0.17±0.03	0.18±0.01
Viscosity (cps)	8.1±0.05	8.2±0.01
pH	5.25	5.10
Folding endurance	105	109

Note: The values presented are arithmetic Mean ±SD's of three determination; C=Complete, D=dried, O=opaque, P=peelable.

Table 3: Effect of formulation on % wound contraction in excision wound model.

Group	Group name	% Wound contraction		
		Day 7	Day 14	Day 21
Group I	Disease Control	17.33±1.35	61.55±0.99	91.67±0.88
Group II	Standard (Silver sulphadiazine)	23.33±1.58	81.0±0.88	99.44±0.11
Group III	Blank	11.22±0.68	75.33±0.51	83.44±0.80
Group IV	Ag FFS	46.56±1.60	89.33±1.58	99.0±0.19
Group V	CuO FFs	37.88±2.50	90.67±0.89	98.89±0.22

Note: the values presented are the arithmetic Mean ±SEM of three determinations.

pH determination

The formulation's pH is comparable to that of the skin, as evidenced by the pH values of 5.25±0.05 for Ag FFS and 5.10±0.01 for Cu FFS. The pH of all FFS is tabulated in Table 2.

Folding Endurance

The folding endurance for Ag FFS and Cu FFS was determined to be 105 and 109 respectively, the findings are shown in Table 2.

Animal activity

Wound healing activity on Albino Wistar rat

To evaluate the developed FFS wound dressing formulation for wound healing activities, a rat skin wound model by excision was used. An incision of 300 mm^2 diameter was produced on the rat's dorsal area and treated for approximately 21 days. The wound area was photographed in both treated and control animals, as shown in Figure 3. The healing process was assessed based on the reduction in the size of the wound area, as shown in Table 3. Excision wound healing model research demonstrates that the formulation given to the test group demonstrated a reduction in wound area from day to day, beginning with the first day of treatment. On the 21st day of therapy, Group I (control) animals exhibited 91.67±0.88% of healing, whereas Group II (standard) animals showed 99.44±0.11% and Group III (blank) mice showed 83.44±0.80%. Group IV (Ag FFS) animals showed 99.0±0.19% healing, whereas Group V (Cu FFS) showed 98.89±0.22% healing.

Determination of period of epithelialization

The epithelization time refers to the moment when a scar has entirely grown. The epithelialization time for group I rats was 17 days, 12 days for group II, 18 days for group III, 16 days for group IV and 15 days for group V.

Histopathology study

After completion of the treatment, the whole wound along with the margins was cut and preserved in 10% buffered formalin to maintain tissue integrity and further the sample was stained, sectioned and embedded. The histopathology images of the grouped animals are shown in Figure 4 (A-E).

Stability Studies

Stability testing was performed in accordance with ICH criteria to ensure the product's quality in various environmental conditions such as temperature and humidity. This study was conducted at these temperatures (4 ± 2°C, 25 ± 2°C and 40°C ± 2°C) and 75% ± 5 relative humidity for three months. The results in Table 4 reveal that there were no significant changes in physical appearance, pH or viscosity.

DISCUSSION

In this work, a polymeric FFS integrated with Ag NPs and CuO NPs was effectively developed for wound healing applications. The potential of this formulation as an advanced wound dressing is supported by the successful synthesis and optimization of the NPs, their incorporation into a stable film-forming system, and the subsequent demonstration of significant wound healing efficacy in an animal model.

In Ag NPs synthesis by the chemical reduction method, Ag ions can be reduced in a PVP solution via two different mechanisms. The first process involves Ag^+ ions coordinating with PVP to produce Ag-PVP complexes (Eq.1). Under alkaline circumstances, these complexes breakdown, and the coordinated Ag^+ species can be reduced by PVP upon heating, resulting in the creation of metallic Ag^0 atoms stabilized by PVP chains (Eq. 2). In the second route, Ag^+ ions combine with hydroxide ions, producing Ag oxide (Ag_2O) as an intermediate (Eq. 3). When heated in the presence of PVP, this oxide is further reduced to metallic Ag^0 NPs, which are sterically stabilized by the PVP matrix (Eq. 4). Reactions can be characterized as follows:

$$1)\ Ag^+ + PVP \longrightarrow Ag\,(PVP)^+$$

$$2)\ Ag\,(PVP)^+ \xrightarrow{\triangle} Ag^0\,(PVP)\downarrow + PVP_{(OX)}$$

$$3)\ 2\,Ag^+ + 2OH^- \longrightarrow Ag_2O\downarrow + H_2O$$

$$4)\ Ag_2O + PVP \xrightarrow{\triangle} 2\,Ag^0\,(PVP)\downarrow + PVP_{(OX)} + H_2O$$

In CuO NPs preparation by the co-precipitation method, when NaOH is added dropwise into the solution, a flocculent precipitation is generated in these blue solutions. The precursor in the blue solution before heat treatment is copper hydroxide [$Cu(OH)_2$]. Copper oxide is obtained after heat treats the Cu $(OH)_2$ precipitation; the reactions can be summarized as follows:

Table 4: Stability studies of Ag FFS and CuO FFS.

4 ± 2°C				25 ± 2°C			40 ± 2°C		
FFS	Physical Appearance	pH	Viscosity (cP)	Physical Appearance	pH	Viscosity (cP)	Physical Appearance	pH	Viscosity (cP)
Ag FFS	No sediment	5.10	8.7±0.2	No visible change	5.22	8.3±0.32	No visible change	5.83	8.1±0.31
Cu FFS	No visible change	5.00	8.8±0.3	No visible change	5.12	8.4±0.17	No visible change	5.9	8.0±0.22

$$1)\ Cu^{2+} + 2NaOH \rightarrow Cu(OH)_2 \downarrow + 2Na^+$$

$$2)\ Cu(OH)_2 \xrightarrow{\triangle} CuO + H_2O$$

Visual inspection and UV-vis spectroscopy provided early, reliable markers of NP development. The color changes from colorless to reddish for Ag NPs and from bluish-green to black for CuO NPs, are typical indicators of SPR and NPs precipitation, respectively. The significant SPR peak at 432 nm for Ag NPs and the absorption maximum at 262.5 nm for CuO NPs correspond to recognized literature values, providing strong evidence for the effective production of both types of NPs. Optimization experiments demonstrated that parameters such as precursor concentration, pH, and temperature had a significant impact on the NPs' yield, size, and stability. For Ag NPs, a concentration of 7 mM $AgNO_3$, pH 11, and a temperature of 60°C were found to be ideal, creating NPs with high yield and smaller size, as indicated by the blue shift in SPR wavelength as concentration increased. A common finding was that after synthesis of Ag NPs at various concentrations, the color of the samples progressively changed from yellow to dark reddish brown, with the intensity of the color increasing as the concentration of Ag salt rose. The primary study demonstrates that when the concentration of $AgNO_3$ increases, the absorption intensity increases, resulting in the creation of more Ag NPs. The UV-Vis spectra exhibited maximum absorbance at 436 nm, 431.05 nm, and 424.19 nm for 5 mM, 6 mM, and 7 mM, respectively, Figure 1 (C). When the precursor concentration was raised, there was a little blue shift in the SPR wavelength, suggesting that the mean particle diameter of the synthesized Ag NPs had decreased. The highest yield of Ag NPs was found when the concentration of $AgNO_3$ solution was 7 mM, which is also in agreement with an earlier study.[36] As a result, 7 mM is regarded as the optimal concentration for Ag NP production. According to the UV-Vis spectra of effect of pH, Figure 1 (E), no absorption peak was detected in the 400-600 nm range for the sample at pH 7. At pH 8, an absorption band developed at about 415 nm, suggesting that Ag NPs were formed. As the pH increased, a blue shift occurred from 418 nm to 415 nm. It was discovered that the absorption peak intensity steadily increased with increasing pH, implying that the reduction rate of Ag ions rises with pH. At lower pH, bigger Ag NPs are generated, whereas at higher pH, smaller and more distributed Ag NPs are created. This observation was consistent with an earlier study.[37] Thus, pH 11 was chosen as the ideal pH. The UV spectra of effect of temperature on Ag NPs, shown in Figure 1 (G). The results indicated that somewhat increased temperatures expedited the reduction process, which had dropped from 80°C. Since a considerable drop in peak intensity was seen at 80°C, Hence, 60°C was chosen as the optimal temperature for Ag NPs synthesis. A similar result was reported earlier.[38]

The greatest absorbance intensity for CuO NPs was observed at a concentration of 0.3 M and a pH of 12, indicating optimum synthesis. The adsorption peak shown in Figure 1(D) demonstrated that as concentration of precursor progressed, the absorption edge migrated slightly towards shorter wavelengths, and peak strength increased proportionally. The rise in peak intensity indicates the higher yield of NPs. As a result, the optimal concentration for CuO NP synthesis was determined to be 0.3 M. According to literature, as the pH rises, particle size reduces, but the surface-to-volume ratio rises.[39] The constant form of the absorbance curves and the lack of a peak shift indicate that particle size stays generally stable over the pH range, but the rise in absorbance intensity represents greater nanoparticle

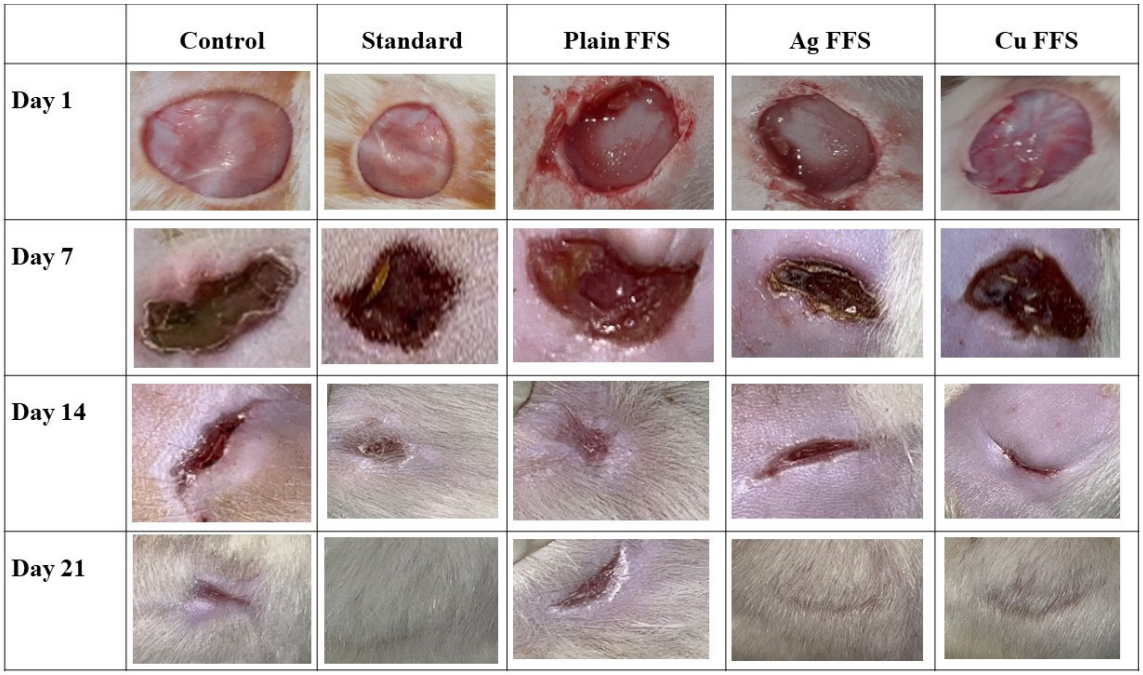

Figure 3: Photographs of Wound healing on animal model.

concentration. Thus, pH 12 was chosen as the optimal pH, Figure 1 (F). The temperature analysis found that 90°C resulted in increased yield and possibly better crystallinity for CuO NPs without substantial size change. This trend indicates a larger yield of CuO NPs at higher temperatures, most likely due to increased nucleation and particle formation rates aided by increased thermal energy. The spectra exhibited absorption between 250-300 nm, which is typical for CuO owing to interband electronic transitions. There was no substantial peak shift, indicating that particle size remained essentially consistent throughout temperatures, Figure 1 (H). These improved conditions were critical for creating NPs with desirable characteristics for later characterization.

The lack of nitrate peaks in the FT-IR spectra of the final Ag NPs compared to the $AgNO_3$ precursor demonstrated that the Ag+ ions had been completely reduced. The observed spectrum changes in PVP's C=O and O-H/N-H bands after NP creation show that the polymer successfully coordinated and capped the NPs, which is critical for avoiding aggregation and guaranteeing colloidal stability. The sol-gel synthesis of CuO NPs was verified by the elimination of sulphate peaks from the $CuSO_4$ precursor and the emergence of a distinctive Cu-O stretching band approximately 820 cm^{-1} in the end product. These FT-IR results agree with recent publications, indicating the NPs' correct chemical synthesis, Figure 2 (A, B).

The average particle size and PDI showed that the generated Ag NPs and CuO NPs are moderately monodispersed. The electrical potential between the main liquid in which a particle is floating and the inner Helmholtz layer at the particle's surface is known as the zeta potential. It is a parameter that shows the charge of a particle and offers details about the possible stability of the colloidal system. Particles in suspension repel one another and do not flocculate if they all have a strong negative or positive zeta potential. On the other hand, there is little force preventing the particles from clumping together and flocculating if their zeta potential levels are low. The Zeta potential values NPs indicate that the manufactured NPs are moderately stable and likely to form aggregates. SEM pictures of Ag NPs, Figure 2 (C), reveal that they are smaller, spherical, non-uniform, and clustered. The diameters are in the nanoscale range (90-130 nm), which is consistent with the particle size measurements reported earlier. The SEM picture of the produced CuO NPs, Figure 2 (D) exhibits an irregular, almost spherical shape with particle sizes ranging from 202 to 356 nm. The particles seem agglomerated, indicating minimal interparticle repulsion and the potential lack of capping agents. Antimicrobial effectiveness, an essential feature for wound dressings, was established using MIC testing. This validates the lowest NPs concentration necessary to suppress observable microbial growth. *E. coli* and *S. aureus* were both suppressed by each NP, indicating broad-spectrum activity.

The FFS formulation with Eudragit L100 and HPC was successfully developed with incorporation of NPs resulting in films with desirable qualities such as adequate drying time, flexibility, thickness, pH near skin pH, good spreadability, and great folding durability. These features are critical for patient compliance, ease of application, and maintaining close contact with the wound bed for optimal drug delivery. The essential prerequisite for film-forming polymeric solutions is *in situ* film formation since the liquid may not stay in place for an extended amount of time, reducing the amount of time the medication comes into contact with the wound. The concentration of the polymer and the kind of solvent determine how the film forms. It is crucial to ascertain if the created film is entire or partial, homogeneous or non-sticky, dry, and clear or opaque after the formulation has been poured. Both the films were formed completely, dried, opaque in nature and easily peelable. Since there is a relationship between drying time and film formation. The amount of time needed for the film-forming polymeric solution to completely evaporate its solvent and leave behind a residual film is known as the drying time. It is dependent on the solvent type and polymer content. The formulation is meant to dry on the skin rapidly so that patients don't have to wait a long time. Both formulas demonstrated acceptable drying times and adequate residual film formation, as recorded in Table 2. Due to their strong attachment ability and lack of breaking, the resulting films from both formulations were flexible. The polymer concentration determines the film's thickness. While thin coatings caused peeling issues and made removal more difficult, thick films had the potential to produce cracks. Therefore, the ideal thickness is needed, which may be achieved by using the appropriate amount of polymer. In Table 2, the thickness of the produced films is listed. The findings show that when the polymer content rises, so does the film's thickness and viscosity. In general, the viscosity demonstrates the uniformity of the formulation. The concentration of the polymer has the most impact on viscosity and thickness. A high polymer content will result in a thick formulation consistency and pouring issues. In contrast, a low viscosity solution may offer more FFS and need less contact time since it may flow more readily. Table 2 displays the findings. The pH of both the FFS was in the range was skin's pH, depicting no irritation on skin. The folding endurance values for Ag FFS and Cu FFS was found to be above 100, respectively. This implies that both films have high mechanical strength and flexibility; the findings are shown in Table 2.

The *in vivo* wound healing trial gave the strongest evidence of the formulation's efficacy. By day 21, both the Ag FFS and CuO FFS treatment groups (Groups IV and V) had wound contraction percentages of 99.0% and 98.89%, respectively, which were equivalent to the standard silver sulfadiazine group (99.44%). The epithelization period was likewise shorter in the treatment groups (16 and 15 days) than in the control (17 days). Histopathological examination revealed more details about the mechanism of action. Although the control group samples had full re-epithelization, histopathological analysis showed a healing process with a lingering inflammatory phase. Figure 4 (A) Control

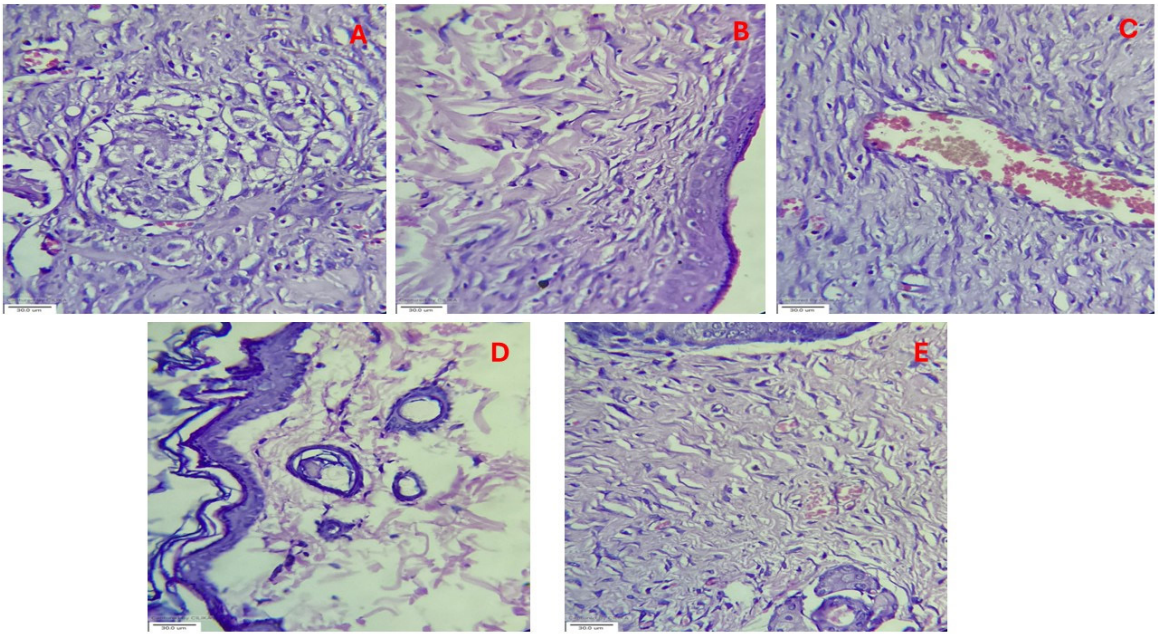

Figure 4: Histopathology images of (A) Control, (B) Standard, (C) Blank FFS, (D) Ag FFS and (E) CuO FFS.

group showed no signs of adnexal regrowth. When taken together, these metrics show that a considerable inflammatory response prolongs the normal, unaided healing response. In contrast to the control group, the standard group demonstrated a more sophisticated and hygienic healing process. Similar to the control, re-epithelialization was complete, although there was a noticeable decrease in the inflammatory response. Mild macrophages with almost full collagen are shown in Figure 4 (B). The blank group demonstrated identical healing to the control group, with full re-epithelialization and mild inflammation. Figure 4 (C) depicts moderate Congestion, a sign of inflammation. The Ag treatment group had a substantially advanced healing response that was unique from the other groups. Re-epithelialization was complete, resulting in full epidermal covering. Notably, the inflammatory phase was completely healed, since there was little congestion, no edema, or inflammatory infiltration, and there were no neutrophils, lymphocytes, macrophages, or large cells, Figure 4 (D). This sample has a similar profile to the control, but with significantly better features. Re-epithelization was completed. Due to significant congestion, inflammation was milder than in the control, as seen in Figure 4 (E). The lymphocytes and macrophages are weak, and there are no neutrophils or large cells. Mild adnexal regeneration occurs; however, it is less pronounced than in standard and Ag FFS. It performs at an intermediate level.

Finally, stability testing done in accordance with ICH recommendations showed that both Ag FFS and CuO FFS were stable over three months under accelerated circumstances (40°C/75% RH), with no notable changes in physical appearance, pH, or viscosity. As a result, no signs of deterioration of the prepared FFS were noticed. This guarantees that the formulation retains its purity and efficacy over an acceptable shelf life.

CONCLUSION

In the present study, an attempt was made to prepare FFS incorporated with Ag NPs and CuO NPs with the aim of experimenting *in vivo* wound healing activity in Albino Wistar rats. From the research findings, it may be concluded that: Ag NPs were prepared via a chemical reduction method, using $AgNO_3$, NaOH and PVP, whereas CuO NPs were synthesized using a sol–gel technique, by using NaOH and $CuSO_4.5H_2O$ as precursor. Both NPs exhibited strong absorption peaks, and their synthesis was systematically optimized with respect to precursor concentration, pH, and temperature. FT-IR spectra revealed characteristic functional group interactions consistent with previous reports and the prepared NPs showed compatibility with the excipients used. Comprehensive characterization confirmed their nanoscale dimensions and desirable physicochemical properties. Particle size analysis indicated nanoparticles within the nanometre range with monodisperse distribution. Zeta potential measurements suggested moderate stability. SEM imaging, though not highly defined, still provided insight into their morphology: Ag NPs showing clusters with some spherical particles, and CuO NPs displaying a predominantly spherical structure, with uneven shape. Antibacterial assessment through MIC revealed broad-spectrum activity of both NPs against *Staphylococcus aureus* and *Escherichia coli*. Following characterization, these optimized NPs were incorporated into polymeric FFS, prepared using Eudragit L 100 and HPC. The formulations were evaluated for their physicochemical attributes and further subjected to *in-vivo* wound healing studies using Wistar rat models. Both Ag FFS and CuO FFS formulations demonstrated significant wound contraction and histopathological evidence of tissue regeneration, thereby confirming their therapeutic potential.

FUTURE PERSPECTIVES

The outcomes of this research highlight NPs incorporated into FFS as a promising platform for advanced wound management. By integrating antibacterial activity with accelerated wound closure, these formulations hold considerable potential not only for clinical dermatology but also for cosmeceutical applications. Further studies focusing on long-term safety, large-scale production, and clinical translation are warranted to advance this approach toward real-world therapeutic use.

SUMMARY

In healthcare, managing wounds effectively is still a major concern, especially in light of the growing risk of antimicrobial resistance linked to traditional drug-based treatments. In order to promote topical wound healing, this work investigates a new drug-free method that incorporates Ag and CuO NPs into a polymeric FFS. The NPs were produced and tuned for critical physicochemical properties to assure stability and bioactivity, and their incorporation into the FFS sought to offer prolonged and regulated engagement with the wound surface. The study underscores the necessity of creating antimicrobial techniques that decrease dependence on standard antibiotics, giving a mechanism to enhance natural wound healing processes while lowering the danger of resistance development. By merging nanotechnology with polymeric film systems, this study proposes a potentially safe, adaptable, and effective platform for topical wound care, setting the framework for future research into non-drug-based therapeutic interventions in tissue healing and regenerative medicine.

ACKNOWLEDGEMENT

The authors gratefully acknowledge the Institutional Animal Ethics Committee of Maratha Mandal's College of Pharmacy, Belagavi, Karnataka, India, for approving this study (Approval No. MMCP/2024-25/B.Ph/218). We thank Central Research Laboratory, Belagavi, Karnataka, for providing animal house for conducting the experiment as well as the staff for their assistance in animal care, and for providing essential facilities and infrastructure.

ABBREVIATIONS

Ag: silver, **CuO:** copper oxide, **NPs**: nanoparticles **FFS:** film forming solution, **PVP:** polyvinyl pyrollidione K25, **NaOH:** Sodium hydroxide, **$AgNO_3$:** silver nitrate, **$CuSO_4.5H_2O$:** Copper sulphate pentahydrate, **FT-IR:** Fourier transforms infrared spectroscopy, **DLS:** Dynamic Light Scattering, **SEM:** Scanning Electron Microscope, **MIC:** Minimum Inhibitory Concentration, **HPC:** Hydroxy Propyl Cellulose, **SPR:** Surface Plasmon Resonance. **IAEC:** Institutional Animal Ethics Committee, **UV-Vis:** Ultraviolet-visible, **PDI:** Polydispersity Index, **ICH:** International Council for Harmonization of Technical Requirements for Pharmaceuticals for Human Use.

CONFLICT OF INTEREST

The authors declare that there is no conflict of interest.

FUNDING

This work was supported by the Deanship of Scientific Research, Vice Presidency for Graduate Studies and Scientific Research, King Faisal University, Saudi Arabia [Grant No. KFU254540].

AUTHOR CONTRIBUTION

Ketura Kambampaty: Writing-original draft, Methodology, Data curation. **Nagesh C:** Conceptualization, Validation of experimental work, **Suma Naduvinamani:** Supervision, Visualization. **Kartik Khot:** Visualization, **Sibghatullah Muhammad Ali Sangi:** Visualization, **Sreeharsha Nagaraja:** Visualization, **Girish Meravanige:** Visualization, **Monirul Islam:** Funding acquisition, Writing- review and editing, **Pavan Kumar Sreenivasalu:** Visualization, **Shahzad Chohan:** Visualization.

REFERENCES

1. Lopez-Ojeda W, Pandey A, Alhajj M. Anatomy, skin (integument) [Internet]. Treasure Island, FL: StatPearls Publishing; 2024 Jan. [cited Dec 5 2025] Available from: https://www.ncbi.nlm.nih.gov/books/NBK441980/.
2. Ozgok Kangal MK, Kopitnik NL. Treasure Island, FL: StatPearls Publishing; 2025 Jan. Physiology, Wound Healing [Internet]. [cited Dec 5 2025] Available from: https://www.ncbi.nlm.nih.gov/books/NBK518964/.
3. Lindholm C, Searle R. Wound management for the 21st century: combining effectiveness and efficiency. Int Wound J. 2016; 13 Suppl 2:5-15. doi: 10.1111/iwj.12623, PMID 27460943.
4. Subramaniam T, Fauzi MB, Lokanathan Y, Law JX. The role of calcium in wound healing. Int J Mol Sci. 2021;22(12):6486. doi: 10.3390/ijms22126486, PMID 34204292.
5. Wang H, Xu Z, Li Q, Wu J. Application of metal-based biomaterials in wound repair. Engineered Regen. 2021;2:137-53. doi: 10.1016/j.engreg.2021.09.005.
6. Talapko J, Matijević T, Juzbašić M, Antolović-Požgain A, Škrlec I. Antibacterial activity of silver and its application in dentistry, cardiology and dermatology. Microorganisms. 2020;8(9):1400. doi: 10.3390/microorganisms8091400, PMID 32932967.
7. Sandoval C, Ríos G, Sepúlveda N, Salvo J, Souza-Mello V, Farías J. Effectiveness of copper nanoparticles in wound healing process using *in vivo* and *in vitro* studies: a systematic review. Pharmaceutics. 2022;14(9):1838. doi: 10.3390/pharmaceutics14091838, PMID 36145586.
8. Carrillo-Carrión C, Nazarenus M, Paradinas SS, Carregal-Romero S, Almendral MJ, Fuentes M, *et al.* Metal ions in the context of nanoparticles toward biological applications. Curr Opin Chem Eng. 2014;4:88-96. doi: 10.1016/j.coche.2013.11.006.
9. Nandhini J, Karthikeyan E, Rajeshkumar S. Nanomaterials for wound healing: current status and futuristic frontier. Biomed Technol. 2024;6:26-45. doi: 10.1016/j.bmt.2023.10.001.
10. Shumbula NP, Ndala ZB, Nkabinde SS, Mente P, Mpelane S, Shumbula MP, *et al.* Dopamine capped silver/copper bimetallic elongated nanoparticles and their potential application in wound healing. Next Nanotechnol. 2024;6:100077. doi: 10.1016/j.nxnano.2024.100077.
11. Zhou W, Zi L, Cen Y, You C, Tian M. Copper sulfide nanoparticles-incorporated hyaluronic acid injectable hydrogel with enhanced angiogenesis to promote wound healing. Front Bioeng Biotechnol. 2020;8:417. doi: 10.3389/fbioe.2020.00417, PMID 32457889.
12. Dalisson B, Barralet J. Bioinorganics and wound healing. Adv Healthc Mater. 2019;8(18):e1900764. doi: 10.1002/adhm.201900764, PMID 31402608.
13. Borbolla-Jiménez FV, Peña-Corona SI, Farah SJ, Jiménez-Valdés MT, Pineda-Pérez E, Romero-Montero A, *et al.* Films for wound healing fabricated using a solvent casting technique. Pharmaceutics. 2023; 2023(Jul 9):1914. doi: 10.3390/pharmaceutics15071914, PMID 37514100.
14. Deutsch CJ, Edwards DM, Myers S. Wound dressings. Br J Hosp Med (Lond). Wound Management for the 21st Century [Internet]. London. 2017;78(7):C103-9. doi: 10.12968/hmed.2017.78.7.C103, PMID 28692373.

15. Rahmanian E, Tanideh N, Karbalay-Doust S, Mehrabani D, Rezazadeh D, Ketabchi D, *et al.* The effect of topical magnesium on healing of pre-clinical burn wounds. Burns. 2024;50(3):630-40. doi: 10.1016/j.burns.2023.10.015, PMID 37980271.
16. El-Shamy OA, El-Adawy MM, Abdelsalam M. Chemical synthesis of a polyvinylpyrrolidone-capped silver nanoparticle and its antimicrobial activity against two multidrug-ResistantAeromonas species. Aquacult Res. 2023;2023(1):3641173. doi: 10.1155/2023/3641173.
17. Banu T, Jamal M, Gulshan F. Opto-structural properties and photocatalytic activities of CuO NPs synthesized by modified sol–gel and Co-precipitation methods: a comparative study. Results Mater. 2023;19:100419. doi: 10.1016/j.rinma.2023.100419.
18. Marinescu L, Ficai D, Ficai A, Oprea O, Nicoara AI, Vasile BS, *et al.* Comparative antimicrobial activity of silver nanoparticles obtained by wet chemical reduction and solvothermal methods. Int J Mol Sci. 2022 May 26;23(11): 5982. doi: 10.3390/ijms23115982, PMID 35682664.
19. Bakil SN, Kamal H, Abdullah HZ, Idris MI. Sodium alginate-zinc oxide nanocomposite film for antibacterial wound healing applications. Biointerface res. J Appl Chem. 2020;10(2):6245-52.
20. Dasaradhudu Y, Arunachalam Srinivasan MA. Synthesis and characterization of silver nano particles using co-precipitation method. Mater Today Proc. 2020;33:720-3. doi: 10.1016/j.matpr.2020.06.029.
21. Manuja A, Kumar B, Chhabra D, Brar B, Thachamvally R, Pal Y, *et al.* Synergistic effect of zinc-chitosan nanoparticles and hydroxychloroquine to inhibit buffalo coronavirus. Polymers. 2023;15(13):2949. doi: 10.3390/polym15132949, PMID 37447594.
22. Chikezie IO. Determination of minimum inhibitory concentration (MIC) and minimum bactericidal concentration (MBC) using a novel dilution tube method. Afr J Microbiol Res. 2017;11(23):977-80. doi: 10.5897/AJMR2017.8545.
23. Chikezie IO. Determination of minimum inhibitory concentration (MIC) and minimum bactericidal concentration (MBC) using a novel dilution tube method. Afr J Microbiol Res. 2017;11(23):977-80. doi: 10.5897/AJMR2017.8545.
24. Umar AK, Butarbutar M, Sriwidodo S, Wathoni N. Film-forming sprays for topical drug delivery. Drug Des Dev Ther. 2020;14:2909-25. doi: 10.2147/DDDT.S256666, PMID 32884234.
25. Kittaneh M, Qurt M, Malkieh N, Naseef H, Muqedi R. Preparation and evaluation of vitamin D3 supplementation as transdermal film-forming solution. Pharmaceutics. 2022;15(1):39. doi: 10.3390/pharmaceutics15010039, PMID 36678668.
26. Chamsai B, Soodvilai S, Opanasopit P, Samprasit W. Topical film-forming chlorhexidine gluconate sprays for antiseptic application. Pharmaceutics. 2022;14(6):1124. doi: 10.3390/pharmaceutics14061124, PMID 35745696.
27. Cebrian RA, Dalmagro M, Pinc MM, Donadel G, Engel LA, Bariccatti RA, *et al.* Development and characterization of film-forming solution loaded with *Syzygium cumini* (L.) Skeels for topical application in post-surgical therapies. Pharmaceutics. 2024;16(10):1294. doi: 10.3390/pharmaceutics16101294, PMID 39458623.
28. Shetty A, Dubey A, Chrystle J, John A, Das P, Hebbar S. Fabrication and *in vitro* characterization of curcumin film-forming topical spray: an integrated approach for enhanced patient comfort and efficacy. F1000Research. 2024;13:138.
29. Kumar PT, Abhilash S, Manzoor K, Nair SV, Tamura H, Jayakumar R. Preparation and characterization of novel β-chitin/nanosilver composite scaffolds for wound dressing applications. Carbohydr Polym. 2010;80(3):761-7. doi: 10.1016/j.carbpol.2009.12.024.
30. Sabat PK, Pradhan SP, Patro RA. Evaluation of excisional and incisional wound healing activity of electrohomeopathic drug (spagyric essence) green electricity in rats. Int J Pharm Pharm Sci. 2020;12(10):72-5. doi: 10.22159/ijpps.2020v12i10.38674.
31. Jafar M, Ashwlayan VD. The evidence based wound healing activity of herbal plant Populus deltoides on Albino Wistar Rats. Res J Pharm Technol. 2025;18(4):1590-6. doi: 10.52711/0974-360X.2025.00228.
32. Babu PJ, Doble M, Raichur AM. Silver oxide nanoparticles embedded silk fibroin spuns: microwave mediated preparation, characterization and their synergistic wound healing and anti-bacterial activity. J Colloid Interface Sci. 2018;513:62-71. doi: 10.1016/j.jcis.2017.11.001, PMID 29132106.
33. Vij SRB. Formulation, development and evaluation of film-forming gel for prolonged dermal delivery of terbinafine hydrochloride. Int J Pharm Sci Res. 2014;5(09):537.
34. Chicea D, Nicolae-Maranciuc A, Doroshkevich AS, Chicea LM, Ozkendir OM. Comparative synthesis of silver nanoparticles: evaluation of chemical reduction procedures, AFM and DLS size analysis. Materials (Basel). 2023;16(15):5244. doi: 10.3390/ma16155244, PMID 37569948.
35. Kumar N, Parui SS, Limbu S, Mahato DK, Tiwari N, Chauhan RN. Structural and optical properties of sol–gel derived CuO and Cu2O nanoparticles. Mater Today Proc. 2021;41:237-41. doi: 10.1016/j.matpr.2020.08.800.
36. Susilowati E, Mahardiani L, Ariani SR, Sulaeman IM. Synthesis, optimization and antibacterial performance of colloidal silver nanoparticles in chitosan. Indones J Chem. 2023;23(6):1652-63. doi: 10.22146/ijc.84822.
37. Marciniak L, Nowak M, Trojanowska A, Tylkowski B, Jastrzab R. The effect of pH on the size of silver nanoparticles obtained in the reduction reaction with citric and malic acids. Materials (Basel). 2020;13(23):5444. doi: 10.3390/ma13235444, PMID 33260479.
38. Jiang XC, Chen WM, Chen CY, Xiong SX, Yu AB. Role of temperature in the growth of silver nanoparticles through a synergetic reduction approach. Nanoscale Res Lett. 2010;6(1):32. doi: 10.1007/s11671-010-9780-1, PMID 27502655.
39. Rajesh KM, Ajitha B, Ashok Kumar Reddy Y, Suneetha Y, Sreedhara Reddy P. Synthesis of copper nanoparticles and role of pH on particle size control. Mater Today Proc. 2016;3(6):1985-91. doi: 10.1016/j.matpr.2016.04.100.

Cite this article: Kambampaty K, Setty NC, Naduvinamani S, Khot KB, Sangi SMA, Nagaraja S, *et al*. Experimental Research of Ions in Wound Healing Via Film Forming Solution. Indian J of Pharmaceutical Education and Research. 2026;60(2s):s687-s698.